Hyperlocal Variation in Soil Iron and Rhizosphere Microbiome Determines Disease Development in Amenity Turfgrass

Ming-Yi Chou#, Smita Shrestha, Renee Rioux, Paul Koch

Department of Plant Pathology, University of Wisconsin-Madison, Madison, Wisconsin, USA

Running Head: Soil Microbiome and Dollar Spot

#Address correspondence to Ming-Yi Chou, mchou5@wisc.edu

Main body of text: 4970 words

Abstract: 385 words

ABSTRACT

Dollar spot, caused by the fungal pathogen *Clarireedia spp.*, is an economically important disease of amenity turfgrass in temperate climates worldwide. This disease often occurs in a highly variable manner, even on a local scale with relatively uniform environmental conditions. The objective of this study was to investigate mechanisms behind this local variation, focusing on contributions of the soil and rhizosphere microbiome. Turfgrass, rhizosphere, and bulk soil samples were taken from within a 256 m^2 area of healthy turfgrass, transported to a controlled environment chamber, and inoculated with *C. jacksonii*. Bacterial communities were profiled targeting the 16s rRNA gene, and 16 different soil chemical properties were assessed. Despite their initial uniform appearance, the samples differentiated into highly susceptible and moderately susceptible groups following inoculation in the controlled environment chamber. The highly susceptible samples harbored a unique rhizosphere microbiome with lower relative abundance of antibiotic-producing bacterial taxa and higher predicted abundance of genes associated with xenobiotic biodegradation pathways. In addition, stepwise regression revealed that bulk soil iron content was the only significant soil characteristic that positively regressed with decreased dollar spot susceptibility during the peak disease development stage. These findings suggest that localized variation in soil iron induces the plant to select for a particular rhizosphere microbiome that alters the disease outcome. More broadly, further research in this area may indicate how plot-scale variability in soil properties can drive variable plant disease development through alterations in the rhizosphere microbiome.

IMPORTANCE

Dollar spot is the most economically important disease of amenity turfgrass, and more fungicides are applied targeting dollar spot than any other turfgrass disease. Dollar spot symptoms are small (3-5 cm), circular patches that develop in a highly variable manner within plot-scale even under seemingly uniform conditions. The mechanism behind this variable development is unknown. This study observed that differences in dollar spot development over a 256 m^2 area were associated with differences in bulk soil iron concentration and correlated with a particular rhizosphere microbiome. These findings provide important clues for understanding the mechanisms behind the highly variable development of dollar spot, which may offer important clues for innovative control strategies. Additionally, these results also suggest that small changes in soil properties can alter plant activity and hence the plant-associated microbial community which has important implications for a broad array of important agricultural and horticultural plant pathosystems.

INTRODUCTION

Dollar spot on cool-season turfgrasses in North America is caused by the fungus *Clarireedia jacksonii* and is the most economically important disease of amenity turfgrass in temperate climates around the world (1). It causes roughly circular patches of bleached turfgrass 3 to 5 cm in diameter that can blight the stand and reduce the functionality of the site for recreational purposes (2). The primary host of dollar spot is creeping bentgrass (*Agrostis stolonifera*), and a lack of host resistance or effective cultural control strategies has made dollar spot the target of more fungicide applications than any other turfgrass disease (3). Heavy reliance on synthetic fungicides has led to the development of fungicide resistant fungal populations (4), imposes a significant financial burden on the turfgrass manager (5), and increases the risk of human and

environmental contamination resulting from repeated chemical exposures (6). The development of dollar spot symptoms is often highly variable within several meters distance, even in uniformly managed turfgrass with nearly identical environmental conditions (7). While it is not known why dollar spot symptoms develop in such a variable manner, one plausible explanation is a link to hyperlocal variations in microbial antagonists or variations in soil physical, chemical, or biological properties.

Spatial variation in plant disease is often observed in both managed and natural plant systems, and most studies on variation in plant disease incidence and severity have been conducted in large-scale agricultural fields over tens or hundreds of hectares. A. Adiobo et al. (8) observed that the physicochemical and microbial properties of andosols suppressed *Pythium myriotylum* root rot in cocoyam (*Xanthosoma sagittifolium*) more effectively than ferralsols. Varied susceptibility to disease in adjacent fields with similar soil physicochemical characteristics has commonly been attributed to disease suppressive or disease conducive soils and is often influenced by cropping history (9, 10). Though on a larger scale than the variation observed in dollar spot, the pathogen suppression function of a specific suppressive soil has provided some clues as to how the same soil type could have dramatically different pathogen suppression functions. Enrichment of the antagonistic microbial population in the rhizosphere often serves as the key plant pathogen suppression mechanism in previously characterized disease suppressive soils (11). As a classic example, enriched antibiotic 2,4-diacetylphloroglucinol-producing fluorescent *Pseudomonas* species led to a reduction in take-all disease when found in the rhizosphere of wheat and flax (12).

The rhizosphere microbiome and its functions are co-determined by both the plant and the soil. The host plant produces root exudates that recruit particular microbes from within the soil (11).

The soil harbors varied microbial communities shaped by soil type and associated properties, such as structure and pH (13). Therefore, the rhizosphere microbiome and its microbial disease suppressive function can shift following changes in the soil environment. H. Peng et al. (14) varied the chemical and physical properties of *Fusarium oxysporum* f. sp. *cubense* suppressive and conducive soils and showed that soil physicochemical traits can mediate suppressiveness of both suppressive and conducive soils against the pathogen's chlamydospores. This suggests that soil physicochemical and microbial properties can cooperatively affect plant disease suppression in agricultural fields.

Soil spatial variation in microbial properties is often studied at multiple levels, including micro, plot, field, landscape and regional scales (15, 16). Over a small plot-scale, spatial variation of smut disease (*Ustilago syntherismae*) on crabgrass (*Digitaria sanguinalis*) was influenced by both pathogen spore density and spatial location (17). However, soil property influences were not investigated in this study and spores or other long-distance dispersal mechanisms have never been associated with dollar spot in a field environment (2). High spatial variations in soil physicochemical and microbial properties were observed in a managed grassland, including a wide range of soil pH, nitrogen content, microbial biomass, and microbial catabolism profiles within the scales of several centimeters to meters (18), but the impact of these variations on plant-pathogen interactions remained unclear. Recently, Z. Wei et al. (19) examined disease variation in tomato (*Solanum lycopersicum*) and observed that the rhizosphere soil bacterial community effectively predicted the severity of the soil-borne bacterial disease *Ralstonia solanacearum*. Similarly, S. Chen et al. (20) observed differences in rhizosphere bacterial community structure, diversity, acid phosphatase activity, root iron content, and bulk soil calcium and magnesium between healthy and unhealthy blueberry plants (*Vaccinium*

corymbosum). These results again indicate the importance of both soil chemical properties and the rhizosphere microbiome on plant health over a field-scale or smaller. However, it remains unknown whether the rhizosphere and/or bulk soil microbiome impacts the disease severity of a foliar fungal pathogen when interacting with specific soil chemical properties.

In this study, various factors contributing to the localized variation in dollar spot development on monocultured turfgrass was studied. Rhizosphere and bulk soil microbiomes as well as soil chemical properties were examined to determine possible causes for the highly variable spatial nature of dollar spot development. We hypothesized that soil chemical properties and the rhizosphere microbiome are both significant variables in determining dollar spot disease susceptibility in a uniformly managed and monocultured turfgrass system. Turfgrass is an excellent system to study this phenomenon because the high plant density allows for robust sampling over a small scale. The initial 132 cm^2 surface area turfgrass soil plug harbored an estimated 1,200 individual creeping bentgrass plants, and each sub-sample derived from the soil core contained 10 to 15 individual plants. By understanding the factors that drive variation in dollar spot disease development within a plot-scale in a high-density monoculture system, we may discover mechanisms that can be targeted for improved biological management of a number of important plant pathogens.

RESULTS

Dollar spot development. Dollar spot development was measured as decrease of greenness over time in order to standardize the quantification of disease symptoms as lesion shape and color can be difficult to determine with simple visual assessments. The resulting greenness decay curve

129 followed a sigmoidal decay pattern (r=0.9286 and p-value<0.0001) (Fig.1). Disease symptoms
130 initially developed within two days after inoculation (DAI), then increased rapidly over the next
131 four to twelve DAI, before slowing during the saturation phase on 14 to 16 DAI. Substantial
132 differences in symptom severity between samples started showing up on four DAI and
133 differences remained apparent throughout the incubation.

134 **Attributing soil bacterial community difference as a function of disease variability.** Turf
135 samples were grouped into high, medium, and low disease according to the disease severity of
136 each DAI. The bacterial microbiome from rhizosphere and bulk soil associated with each sample,
137 which had been separated prior to inoculation, was then assessed to see if the microbiome
138 structure explained turfgrass responses to *C. jacksonii* inoculation. The rhizosphere bacterial
139 community differed between high and low disease severity groups when categorized based on
140 severity between 4 and 10 DAI according to permutational analysis of variance (PERMANOVA)
141 (Table 1). There were no differences in bacterial community structure found between high and
142 low disease severity groups when categorized according to initial disease development (DAI 0-2)
143 or the disease saturation phase (DAI 12-16). In addition, no differences in the bulk soil bacterial
144 community were found among the disease severity groups throughout the entire incubation
145 (Table 1). The period that the rhizosphere soil microbiome showed differences in structure
146 between the high and low disease groups (4-10 DAI) matched the backslope of the disease
147 development curve (Fig. 1), which suggested that the initial soil rhizosphere microbiome can
148 affect the peak dollar spot development. The samples were then re-categorized according to their
149 disease status during the peak disease development stage (4-10 DAI) to make the peak disease
150 development period as the target of prediction instead of any single day within this period. The
151 samples initially categorized as high disease during the 4 to 10 DAI period never shifted into the

low severity group and vice versa, so the 18 samples naturally broke into two groups except for one sample that stayed in the medium disease group throughout the study and was excluded from further analysis. Further analyses were performed based on breaking the samples into nine highly susceptible (HS) samples and eight moderately susceptible (MS) samples.

Comparison of rhizosphere bacterial communities of highly susceptible and moderately susceptible turfgrass. Two-dimensional principal coordinate analysis showed that distinct bacterial community structures existed between the bulk and rhizosphere soil and between the rhizosphere soil of HS and MS samples (Fig. 2). PERMANOVA statistically confirmed the visual observations of bacterial community composition differences between sample types (Fig. 2a) and susceptibility groups of rhizosphere soil (Fig. 2b). Although the overall rhizosphere bacterial compositions are different between MS and HS turfgrass, the major microbial taxa are identical when analyzed at family and genus levels with less than 20% and more than 75% of the taxa unidentified at each taxonomic level, respectively (Fig. 3). The dominant families identified included *Gemmataceae*, *Pirellulaceae*, *Chitinophagaceae*, *Pedospheraceae*, and *Burkholderiaceae* (Fig. 3a) and the dominant genus' identified included *Flavobacterium*, *Haliangium*, *Chthoniobacter*, *Pirellula*, and *Gaiella* (Fig. 3b). The majority of the rhizosphere soil amplicon sequence variants (ASVs) are shared between the HS and MS turfgrass (8077) with more ASVs being unique to HS (1181) than MS (347) (Fig. 4). Highly susceptible turfgrass samples also had a higher species richness and β-diversity as shown using the Shannon index (Fig. 5).

In the rhizosphere, there were 28 families and 32 genera different in relative abundance between HS and MS samples according to Welch's t-test (Fig. 6a). A balance analysis that accounted for the compositional nature of the dataset was also performed to detect the microbial signature for

discerning the high and low disease rhizosphere bacterial community. The signatures were determined by searching the association between the factor for overall microbiome difference with the bacterial taxa balances defined as normalized log ratio of the geometric mean of the numerator and denominator bacterial taxa. The results showed that relative abundance log ratio of *Rhizobacter* (numerator) to *Microvirga* (denominator) at the genus level and *Solibacteraceae* subgroup3 (numerator) to *Saprospiraceae* (denominator) at the Family level were robust microbial signatures to differentiate the HS and MS turfgrass rhizosphere bacterial community with an adjusted area under the receiver operating characteristic curve for cross-validation equal to 0.9875 and 0.983 for genus and family level, respectively (Fig. 6b).

A co-occurrence network analysis was performed to visualize the microbial interaction of HS and MS turf rhizosphere soil bacteria and showed different network patterns (Fig. 7a). The co-occurrence networks were then further analyzed using "NetShift" to quantify the differences and identify the keystone microbial taxa that triggered the shift of the microbial networking between HS and MS rhizosphere bacterial communities when clustered at the Family and Genus level (Fig. 7b). There were 55 families and 28 genera identified as driver taxa when comparing HS and MS co-occurrence networks aggregated at each taxonomic level.

Rhizosphere soil bacterial function was predicted using Tax4Fun2 (21) to explore the potential microbial functional differences between HS and MS samples during the peak disease development period. Predicted functional pathways at level-two according to KEGG reference for molecular functions of genes (22) including nucleotide metabolism, folding, sorting and degradation, cell motility, translation, transcription, replication and repair, and metabolism of cofactors and vitamins associated genes were found to be more abundant in rhizosphere of MS

197 samples (Fig 8). In the HS samples rhizosphere genes associated with xenobiotic biodegradation
198 and metabolism pathways associated genes were more abundant (Fig. 8).

199 **Bulk soil nutrient and chemical property analysis.** Bulk soil chemical properties were
200 compared among the three disease severity groups categorized according to turf dollar spot
201 severity throughout the incubation period. The bulk soil was sampled prior to the inoculation of
202 *C. jacksonii* to evaluate if bulk soil chemical property explained the turfgrass responses to the
203 pathogen inoculation. The results showed that iron concentration was significantly lower in the
204 high disease than the low disease group throughout the peak disease development stage from 4 to
205 10 DAI (Table 2), and iron was also lower in the HS samples relative to the MS samples
206 (p=0.0021) following re-categorization of the samples (Table S1 in the supplemental material). A
207 Mantel test was conducted to determine correlation between the overall soil chemical properties
208 and the soil bacterial community. Bulk soil chemical properties did not correlate with the bulk
209 soil bacterial community (r=-0.2297, p=0.966) but they did correlate with the rhizosphere
210 bacterial community (r= 0.274, p=0.048). To further examine the relationship between bulk soil
211 chemical properties and dollar spot severity during the peak disease development stage, a
212 backward stepwise regression model was constructed after removing significant colinear
213 variables. The stepwise model (adjusted r^2=0.5041, p=0.002031) suggested that iron significantly
214 (p=0.00062) and positively regressed with average turfgrass greenness during the peak
215 development period (Table 3).

216

217 DISCUSSION

The results from this study indicated that initial differences in the soil rhizosphere bacterial community can predict the level of dollar spot susceptibility in turfgrass plants. These differences occurred over small areas despite uniform host plants and seemingly uniform environmental conditions. The mechanisms of disease suppression provided by the rhizosphere community were not directly studied, but differential analysis of microbial taxa relative abundances, and NetShift analysis of co-occurrence networks in this study provided supporting information for the hypothesis that disease suppression is related to the occurrence of antagonistic organisms in the rhizosphere. A similar hypothesis was also suggested in work done by Z. Wei et al. (19), which indicated that the rhizosphere bacterial community determined occurrence and severity of *Ralstonia solanacearum* in tomato plants and specifically linked disease suppression to the antagonistic activity of soil bacteria in the genera *Bacillus* and *Pseudomonas*. In our study, differential analysis revealed that certain families and genera were higher in relative abundance in the rhizosphere of MS samples compared to HS samples. These families, including *Nocardiaceae* and *Xanthomonadaceae*, and genera, including *Rhodococcus* and *Janthinobacterium*, are known to produce a range of antimicrobial compounds (23-26). Among the microbial co-occurrence network shift drivers identified through "NetShift", node betweenness was significantly increased in MS samples for certain genera, including *Pseudonocardia*, *Streptomyces*, and "*Candidatus Entotheonella*," which are all known for their ability to produce antifungal compounds (27-29). While more research is needed, these findings provide possible explanations for microbial suppression of dollar spot in MS turf samples.

In addition to known antibiotic producers, other bacterial taxa with environmental or plant functional importance in the rhizosphere differed between the HS and MS samples. The balance analysis revealed that the log ratios of *Saprospiraceae* and *Solibacteraceae* subgroup3 at the

family level and *Rhizobacter* to *Microvirga* at the genus level can effectively differentiate between the rhizosphere microbiomes of the HS and MS groups. These results corresponded with differential relative abundance analysis as these taxa of microbial signatures were also captured by the differential relative abundance analyses. Microbial species under the genus *Microvirga* include many root symbionts (30), whereas members of the *Rhizobacter* genus are common rhizobacteria (31) and can also be plant pathogenic (32). Although the relative abundances were low, these identified taxa served as key signatures to differentiate the HS and MS rhizosphere bacterial community and may also have functional importance. For example, the identified family signature *Saprospiraceae* was present at a low level in our study (<1% in relative abundance), but members of the *Saprospiraceae* family are known to break down complex organic compounds in the environment (33) and are also suggested to have functional importance while underrepresented in soil abundance (34). The manner in which these microbial signatures interacted with the pathogen and host plant and whether they can be used for future evaluations of dollar spot suppression requires further research.

Functional prediction was performed to better understand implications of the differences identified in microbiome composition and interaction of HS and MS samples in the absence of a comprehensive metagenomic analysis. The MS rhizosphere microbiome was more enriched in genetic information processing and cellular processes metabolic pathways, whereas HS rhizosphere microbiome was more abundant in predicted xenobiotic biodegradation and metabolism. This result could help explain why the HS rhizosphere microbiome resulted in a more susceptible turfgrass sample. Many chemical compounds, such as salicylic acid (SA) analogs and β-Aminobutyric acid, can induce plant systemic acquired resistance that primes plants to defend against pathogens through activation of SA or abscisic acid (ABA) signaling

pathways (35). Higher predicted abundance in gene associated with xenobiotic biodegradation and metabolism metabolic pathways in the HS rhizosphere microbiome suggested that the microbiome can more actively degrade xenobiotics such as agrochemicals, transformation products and secondary metabolites that either have direct antagonistic effects on pathogen growth, or compounds that have roles in priming plants against pathogens.

In the study by Z. Wei et al. (19), structural and functional differences in the rhizosphere microbiome were found to be the sole factors determining disease severity on tomato. In our study, bulk soil iron concentration predicted the disease susceptibility as well as that of the rhizosphere microbiome and seemed to contribute significantly to dollar spot suppression. S. Gu et al. (36) recently showed that siderophore production as a result of bacterial competition for iron resources in the soil environment strongly mediates *R. solanacearum* activity in the tomato rhizosphere. Specifically, iron-scavenging siderophores produced by nonpathogenic members of the bacterial consortia enhanced the fitness of these nonpathogenic bacteria in the soil environment and suppressed pathogen growth. Further large-scale screening of all major bacterial phylogenetic lineages established a strong positive linkage between inhibitory siderophore production by nonpathogenic bacteria and *R. solanacearum* suppression, indicating that the relative abundance of bacteria that produce pathogen-unusable siderophores in the tomato rhizosphere microbiome served as an effective predictor for disease outcome (37). These studies were done in a soil-borne pathosystem and it is unclear how pathogen-suppressing siderophore producers in the rhizosphere would compete with *C. jacksonii*, which is a foliar pathogen and poor soil saprophyte. Other mechanisms are likely involved, such as iron directly or indirectly neutralizing pathogen activity. For example, G. M. Gadd (38) observed that oxalic acid, a potential virulence factor of *C. jacksonii*, can react with the free iron in the plant-soil

interface and precipitate as crystalline or amorphous solids. Also, in iron-deficient soils, induced bacterial production of the siderophore pyoverdine repressed the expression of plant defense-related genes such as the genes involved in SA and ABA pathways which can lead to a higher plant susceptibility to diseases (39).

Low soil iron can also lead to low iron in the plant tissue. Iron plays multifaceted roles in plant defense mechanisms and plant-pathogen interactions (40). For example, iron serves as a key factor in plant disease defense via numerous regulatory genes involved in microbe response and plant homeostasis, including upregulating the transcription of pathogenesis-related genes and catalyzing the reactive oxygen species when attacked by pathogens (41, 42). Unbalanced iron homeostasis in plants can have serious impacts on disease outcomes. Low iron in *Arabidopsis thaliana* led to more severe *Dickeya dadantii* infection due to less ferritin coding transcript AtFER1, callose deposition, and reactive oxygen species production (43). These collective studies on low soil and plant iron may help explain how lower soil iron in our study can lead to higher dollar spot susceptibility in turf and vice versa, but direct evidence on how soil iron interacts with the turfgrass plant to defend against dollar spot requires further analysis.

Numerous field and *in vitro* studies have shown the beneficial effect of iron in plant disease suppression (44-46), and the beneficial effects of iron are often found in conjunction with a pathogen-suppressive soil microbiome (14, 20). Healthy blueberry (*Vaccinium corymbosum*) plants were found to associate with more diverse rhizosphere bacterial communities and higher iron content in the roots compared with unhealthy plants (20). An *in vitro* study demonstrated that soil Fe-EDDHA amendment has an additive and complementary effect in suppressing Fusarium wilt (*Fusarium oxysporum* f. sp. *cubense*) disease severity in banana (*Musa spp*.) grown in a disease suppressive soil (14). The mechanisms of such a complementary effect of iron

in our study remain unclear, but the Mantel test results suggest that the rhizosphere microbiome was likely mediated by interaction between soil iron levels and turfgrass plants, which in turn impacted disease development.

The rhizosphere microbiome is recruited or expelled from the bulk soil through the production of phytochemicals (47, 48) including many organic acids and secondary metabolites (49). More specifically, previous work by Y. Pii et al. (50) demonstrated that plant iron status had a significant impact on the formation of rhizosphere microbiome structures, possibly via the release of different qualitative and quantitative root exudates. In our study, higher Fe in the bulk soil of MS samples likely induced production of root exudates that then recruited a particular rhizosphere microbiome that was more suppressive to dollar spot development. However, this proposed mechanisms requires significant additional research before it can be used to develop innovative plant disease control strategies.

This study revealed several factors that led to variation in disease development over a small area in amenity turfgrass. Although further research is required before making firm conclusions, our findings suggest that antibiotic-producing members in the rhizosphere microbiome likely played a key role in the dollar spot suppression observed in MS samples. Further, soil iron-plant interactions were possibly a key regulatory factor in the assembly of a suppressive rhizosphere microbiome, and this soil-plant-microbe interaction ultimately resulted in the observed variation in disease development on monocultured turfgrass within a small scale. Future studies on whether the disease suppressive function can be transplanted into a conducive soil, and how turfgrass physiologically mediates root exudates to recruit a disease suppressive rhizosphere microbiome by responding to different levels of soil iron will be critical in further exploring the hypotheses raised by this research.

MATERIALS AND METHODS

Experimental design, sampling scheme and sample preparation. The experiment was conducted on a mature stand of creeping bentgrass (*Agrostis stolonifera* 'Alpha') at the O.J Noer Turfgrass Research Facility in Verona, WI, USA. The turf was grown on a native Troxel silt loam and mowed three times per week at the height of 1.25 cm. Eighteen turfgrass samples and the associated soil were taken using a soil sampler with a 13-cm diameter and a 15-cm depth in a 256 m^2 square plot on Oct. 10^{th}, 2019. The samples were divided into a top layer (the top 7.5 cm) and a bottom layer (7.5 to 15 cm depth) by carefully inserting the soil sampler to the specified depths. Due to the nature of the turfgrass and soil properties, there was hardly any soil without direct contact with roots in the top layer, and rarely root presence in the bottom layer soil. Therefore, we defined the bulk soil as the soil from the bottom layer without direct root contact. The soil samples of each layer were stored separately as turf and bulk soil samples. The turf samples were then used for inoculation experiments after they were sub-sampled for rhizosphere microbiome analysis. Bulk soil samples were sub-sampled from the homogenized bottom layer soil for both microbiome and chemical property analysis. Two, 1-cm diameter subsamples to 5-cm depth containing approximately 10 to 15 individual creeping bentgrass plants were taken from each turf sample for microbiome analysis using a custom-made soil probe. The subsamples from the same turf sample were immediately crushed with a sterile scapula and tweezer, and the soil loosely attached to the root system was separated from plant and rhizosphere soil by aggressively shaking in a sterile glass petri dish, rhizosphere soil remained closely attached to the root was then carefully collected using scapula avoiding the root tissues. The intact turf samples, which the subsamples were taken from, were then inoculated with one milliliter of

dollar spot inoculum using a vaporizer within one hour of sampling. The dollar spot inoculum was created by growing *C. jacksonii on* potato dextrose broth for 72 hrs, rinsing three times in distilled water, and homogenizing in sterile 0.85% saline water in a blender for one minute. The final inoculum had an approximate *C. jacksonii* density of $4.1*10^4$ CFU/ml, as determined by testing with triplicated serial dilutions on potato dextrose agar.

After inoculation, the turf samples were incubated in a growth chamber at 25˚C, 70% relative humidity, and 15 hr photoperiod. Each sample was placed on a sterile filter paper with an individual glass water pan. The turf samples were maintained at 0.5 cm height using sterile scissors, supplied with distilled water through wetting the filter paper, and measured for dollar spot severity every other day for 16 days (Fig. S1 in the supplemental material). Dollar spot severity was assessed by taking digital photos 30 cm directly above the turf surface and counting the percentage of green pixels using imageJ. Bulk soil samples were sent to the Cornell Nutrient Analysis Laboratory (Ithaca, NY) to analyze the chemical properties including pH, organic matter content, and Al, Ca, Cu ,Fe, K, Mg, Mn, Mo, Na, P, S, Zn, C and N content according to procedures outline in B. K. Gugino et al. (51). Briefly, soil were dried in open containers overnight, sieved to remove pebbles and plant tissues, soil organic matter content was measured by dry combustion at 550˚C for two hours, and pH was measured as 1:1 soil to water solution by volume using an automatic pH probe (Lignin, Albuquerque, NM). Soil nutrients were extracted using Morgan's solution and quantified with an Inductively Coupled Argon Plasma Spectrophotometry (Thermo Fisher Scientific, Cambridge, UK).

Library Preparation and short-amplicon sequencing. For each of the bulk soil and rhizosphere soil samples, 0.25 g soil was used for DNA extraction using a DNeasy PowerLyzer PowerSoil kit (Qiagen Inc., Germantown, MD) following the manufacturer's protocol. All

379 extractions were quantified for nucleic acid concentration using a NanoDrop1000 (Thermo
380 Fischer Scientific, Waltham, MA). The PCR was performed according to K. A. Dill-McFarland
381 et al. (52) with minor modifications. Briefly, each reaction contained 5 µL of the DNA template
382 at 10 ng/µL, 12.5 µL Kapa HiFi HotStart ReadyMix, 6.5 µL PCR-grade water, and 0.5 µL of
383 each barcoded forward and reverse primer (53), which targeted the v4 region of the 16S rRNA
384 gene. The thermocycling conditions were 3 min at 95 °C prior to 25 cycles of 30 s at 95 °C, 30 s
385 at 55 °C, and 30 s at 72 °C, with a final step of 5 min at 72 °C. The amplicons were purified
386 using a ZR-96 Zymoclean™ Gel DNA Recovery kit (Zymo Research, Irvine, CA) and
387 normalized with a Mag-Bind® EquiPure Library Normalization Kit (Omega Bio-Tek Inc,
388 Norcross, GA). The amplicons were then pooled and quantified to 4 nM with a Qubit™ dsDNA
389 HS Assay kit (Thermo Fischer Scientific, Waltham, MA). The final pool was sequenced on
390 Illumina MiSeq with a 2x250bp PE Illumina Reagent Kit v2 (Illumina, Inc., San Diego, CA) in
391 the Biotechnology Center at the University of Wisconsin-Madison

392 **Data analysis.** The raw sequences were processed using package "DADA2" in R 3.6.0. Forward
393 and reverse reads were quality filtered according to average quality score and merged. The
394 taxonomy levels associated with each amplicon sequence variant (ASV) was assigned according
395 to SILVA database (v.132) after removing the chimeras. The ASV and taxonomic tables were
396 then exported as .txt files and analyzed using R packages "phyloseq" and "vegan." The reads for
397 each sample were normalized using variance stabilizing transformation with the "DeSeq2"
398 package due to a relatively even reads variation among the samples in the library (54). Microbial
399 compositional differences and correlations were analyzed using Bray-Curtis dissimilarity.
400 Shannon diversity of HS and MS were compared using nonparametric Wilcoxon test in JMP Pro
401 14 (SAS Institute, Cary, NC).

Microbial co-occurrence network of HS and MS samples were constructed using Molecular Ecological Network Analysis (MENA) (55), which uses a Random Matrix Theory (RMT)-based method to predict the microbial interactions and capture the magnitude of the interactions. The nodes and the edge lists were then imported into Gephi 0.9.2 (56) for network visualization. Since the overall ASVs were comprised of approximatly 90% of the ASVs having less than 0.02% of overall reads, ASVs that represent less than 0.02% of the total reads after normalization for each sample were filtered out to make the result more readable. The core community of the HS and MS microbial networks were compared to quantify the rewiring of the taxa in the networks by calculating the of neighborhood shift and change of betweenness for the nodes using NetShift (57). Nodes with the highest degree change among these parameters are considered the driver taxa. When analyzed at family and genus level, the ASVs were aggregated at each taxonomy level to create the edge list. Microbial balance analysis was performed using "selbal" package in R at family and genus level using unnormalized ASV counts, as the compositional nature of the short-amplicon sequencing result and the uneven sequencing depths were both accounted in the analysis (58). Differential relative abundances were analyzed using Welch's t-test at a significance level of $\alpha=0.05$ in using Statistical Analysis of Taxonomic and Functional Profiles (STAMP) (59).

Rhizosphere microbiome functional prediction was performed using an R-based tool Tax4Fun2 (21), which used the sequences of the ASV to blast against the SILVA (v.132) reference genome database to create a metagenome profile. The genetic functions were then assigned by BLASTp against the KEGG KO (22) as a reference database. Differences in functional pathways at level-two were statistically analyzed using Welch's t-test in STAMP. The associations of Bray-Curtis

dissimilarity among bulk soil chemical properties, bulk soil microbiome, and rhizosphere microbiome samples were examined using Mantel test in R.

Soil chemical properties among the disease groups were statistically analyzed with nonparametric Wilcoxon test in JMP Pro 14 (SAS Institute, Cary, NC) and regression with average disease severity of peak disease development stage (4-10 DAI) was performed using a stepwise selection for the optimal predictive model in R. Collinearity variable selection and removal was performed using a customized function vif_func (60) to calculate the variance inflation factor. The best model was constructed with backward selection using a function stepAIC under package "MASS".

Data availability. All the raw sequences generated from this study were deposited at the NCBI Sequence Read Archive and are publicly accessible under the project number of PRJNA642971.

ACKNOWLEDGEMENT

The authors thank Kurt Hockmeyer and Qiwei Lei for assistance in sampling, Joseph Skrlupka and Dr. Garret Suen for assistance in preparation for sequencing, and the UW-Madison CALS Statistical Consulting Lab for providing guidance in statistical analysis.

REFERENCES

1. Salgado-Salazar C, Beirn LA, Ismaiel A, Boehm MJ, Carbone I, Putman AI, Tredway LP, Clarke BB, Crouch JA. 2018. Clarireedia: A new fungal genus comprising four

444 pathogenic species responsible for dollar spot disease of turfgrass. Fungal biology
445 122:761-773.
446 2. Smiley RW, Dernoeden PH, Clarke BB. 2005. Compendium of turfgrass diseases, 3rd
447 edition, vol 1. Am Phytopath Society.
448 3. Kerns JP, Tredway LP. 2013. Advances in turfgrass pathology since 1990. Turfgrass:
449 Biology, Use, and Management 56:733-776.
450 4. Sang H, Hulvey J, Popko Jr JT, Lopes J, Swaminathan A, Chang T, Jung G. 2015. A
451 pleiotropic drug resistance transporter is involved in reduced sensitivity to multiple
452 fungicide classes in S clerotinia homoeocarpa (FT B ennett). Molecular plant pathology
453 16:251-261.
454 5. GCI-Staff. 2015. 2015 State of the Industry Report. GIE Media, Inc.
455 6. Tomer V, Sangha JK, Ramya H. 2015. Pesticide: An appraisal on human health
456 implications. Proceedings of the National Academy of Sciences, India Section B:
457 Biological Sciences 85:451-463.
458 7. Horvath B, Kravchenko A, Robertson G, Vargas Jr J. 2007. Geostatistical analysis of
459 dollar spot epidemics occurring on a mixed sward of creeping bentgrass and annual
460 bluegrass. Crop science 47:1206-1216.
461 8. Adiobo A, Oumar O, Perneel M, Zok S, Höfte M. 2007. Variation of Pythium-induced
462 cocoyam root rot severity in response to soil type. Soil Biology and Biochemistry
463 39:2915-2925.
464 9. Mendes R, Kruijt M, De Bruijn I, Dekkers E, van der Voort M, Schneider JH, Piceno YM,
465 DeSantis TZ, Andersen GL, Bakker PA. 2011. Deciphering the rhizosphere microbiome
466 for disease-suppressive bacteria. Science 332:1097-1100.

10. Schlatter D, Kinkel L, Thomashow L, Weller D, Paulitz T. 2017. Disease suppressive soils: new insights from the soil microbiome. Phytopathology 107:1284-1297.

11. Berendsen RL, Pieterse CM, Bakker PA. 2012. The rhizosphere microbiome and plant health. Trends in plant science 17:478-486.

12. Landa BB, Mavrodi OV, Schroeder KL, Allende-Molar R, Weller DM. 2006. Enrichment and genotypic diversity of phlD-containing fluorescent Pseudomonas spp. in two soils after a century of wheat and flax monoculture. FEMS Microbiology Ecology 55:351-368.

13. Berg G, Smalla K. 2009. Plant species and soil type cooperatively shape the structure and function of microbial communities in the rhizosphere. FEMS Microbiology Ecology 68:1-13.

14. Peng H, Sivasithamparam K, Turner D. 1999. Chlamydospore germination and Fusarium wilt of banana plantlets in suppressive and conducive soils are affected by physical and chemical factors. Soil Biology and Biochemistry 31:1363-1374.

15. Parkin T. 1993. Spatial variability of microbial processes in soil—a review. Journal of environmental quality 22:409-417.

16. Piotrowska A, Długosz J, Namysłowska-Wilczyńska B, Zamorski R. 2011. Field-scale variability of topsoil dehydrogenase and cellulase activities as affected by variability of some physico-chemical properties. Biology and Fertility of Soils 47:101-109.

17. Mas MT, Verdú AM. 2018. Soil spatial distribution in a smut fungus-annual grass interaction: Exploring patterns to understand disease dynamics at plot scale. Fungal ecology 33:40-51.

488 18. Ritz K, McNicol J, Nunan N, Grayston S, Millard P, Atkinson D, Gollotte A, Habeshaw
489 D, Boag B, Clegg C. 2004. Spatial structure in soil chemical and microbiological
490 properties in an upland grassland. FEMS Microbiology Ecology 49:191-205.
491 19. Wei Z, Gu Y, Friman V-P, Kowalchuk GA, Xu Y, Shen Q, Jousset A. 2019. Initial soil
492 microbiome composition and functioning predetermine future plant health. Science
493 advances 5:eaaw0759.
494 20. Chen S, Zhu Y, Shao T, Long X, Gao X, Zhou Z. 2019. Relationship between
495 rhizosphere soil properties and disease severity in highbush blueberry (Vaccinium
496 corymbosum). Applied Soil Ecology 137:187-194.
497 21. Wemheuer F, Taylor JA, Daniel R, Johnston E, Meinicke P, Thomas T, Wemheuer B.
498 2020. Tax4Fun2: prediction of habitat-specific functional profiles and functional
499 redundancy based on 16S rRNA gene sequences. Environmental Microbiome 15:1-12.
500 22. Kanehisa M, Sato Y, Kawashima M, Furumichi M, Tanabe M. 2016. KEGG as a
501 reference resource for gene and protein annotation. Nucleic acids research 44:D457-D462.
502 23. Pantanella F, Berlutti F, Passariello C, Sarli S, Morea C, Schippa S. 2007. Violacein and
503 biofilm production in Janthinobacterium lividum. Journal of applied microbiology
504 102:992-999.
505 24. Chiba H, Agematu H, Kaneto R, Terasawa T, Sakai K, Dobashi K, Yoshioka T. 1999.
506 Rhodopeptins (Mer-N1033), Novel Cyclic Tetrapeptides with Antifungal Activity from
507 Rhodococcus sp. The Journal of antibiotics 52:695-699.
508 25. Woappi Y, Gabani P, Singh OV. 2013. Emergence of antibiotic-producing
509 microorganisms in residential versus recreational microenvironments. British
510 microbiology research journal 3:280.

511 26. Goodfellow M. 2014. Family Nocardiaceae, p 595-650. *In* Rosenberg E, DeLong EF,
512 Lory S, Stackebrandt E, Thompson F (ed), The prokaryotes—Actinobacteria. Springer,
513 Berlin.
514 27. Sen R, Ishak HD, Estrada D, Dowd SE, Hong E, Mueller UG. 2009. Generalized
515 antifungal activity and 454-screening of Pseudonocardia and Amycolatopsis bacteria in
516 nests of fungus-growing ants. Proceedings of the National Academy of Sciences
517 106:17805-17810.
518 28. Oskay M. 2009. Antifungal and antibacterial compounds from Streptomyces strains.
519 African Journal of Biotechnology 8.
520 29. Prapagdee B, Kuekulvong C, Mongkolsuk S. 2008. Antifungal potential of extracellular
521 metabolites produced by Streptomyces hygroscopicus against phytopathogenic fungi.
522 International Journal of Biological Sciences 4:330.
523 30. Radl V, Simoes-Araujo JL, Leite J, Passos SR, Martins LMV, Xavier GR, Rumjanek
524 NGa, Baldani JI, Zilli JE. 2014. Microvirga vignae sp. nov., a root nodule symbiotic
525 bacterium isolated from cowpea grown in semi-arid Brazil. International Journal of
526 Systematic and Evolutionary Microbiology 64:725-730.
527 31. Wei L, Si M, Long M, Zhu L, Li C, Shen X, Wang Y, Zhao L, Zhang L. 2015.
528 Rhizobacter bergeniae sp. nov., isolated from the root of Bergenia scopulosa.
529 International journal of systematic and evolutionary microbiology 65:479-484.
530 32. Goto M, Kuwata H. 1988. Rhizobacter daucus gen. nov., sp. nov., the causal agent of
531 carrot bacterial gall. International Journal of Systematic and Evolutionary Microbiology
532 38:233-239.

533 33. McIlroy SJ, Nielsen PH. 2014. The family saprospiraceae, p 863-889, Prokaryotes.
534 Springer Science+ Business Media.
535 34. Kaminsky R, Morales SE. 2018. Conditionally rare taxa contribute but do not account for
536 changes in soil prokaryotic community structure. Frontiers in microbiology 9:809.
537 35. Conrath U. 2009. Priming of induced plant defense responses. Advances in botanical
538 research 51:361-395.
539 36. Gu S, Yang T, Shao Z, Wang T, Cao K, Jousset A, Friman V-P, Mallon C, Mei X, Wei Z.
540 2020. Siderophore-mediated interactions determine the disease suppressiveness of
541 microbial consortia. mSystems 5.
542 37. Gu S, Wei Z, Shao Z, Friman V-P, Cao K, Yang T, Kramer J, Wang X, Li M, Mei X.
543 2020. Competition for iron drives phytopathogen control by natural rhizosphere
544 microbiomes. Nature Microbiology:1-9.
545 38. Gadd GM. 1999. Fungal production of citric and oxalic acid: importance in metal
546 speciation, physiology and biogeochemical processes, p 47-92, Advances in microbial
547 physiology, vol 41. Elsevier.
548 39. Trapet P, Avoscan L, Klinguer A, Pateyron S, Citerne S, Chervin C, Mazurier S,
549 Lemanceau P, Wendehenne D, Besson-Bard A. 2016. The Pseudomonas fluorescens
550 siderophore pyoverdine weakens Arabidopsis thaliana defense in favor of growth in iron-
551 deficient conditions. plant physiology 171:675-693.
552 40. Verbon EH, Trapet PL, Stringlis IA, Kruijs S, Bakker PA, Pieterse CM. 2017. Iron and
553 immunity. Annual review of phytopathology 55.
554 41. Aznar A, Chen NW, Thomine S, Dellagi A. 2015. Immunity to plant pathogens and iron
555 homeostasis. Plant Science 240:90-97.

556 42. Liu G, Greenshields DL, Sammynaiken R, Hirji RN, Selvaraj G, Wei Y. 2007. Targeted
557 alterations in iron homeostasis underlie plant defense responses. Journal of Cell Science
558 120:596-605.
559 43. Kieu NP, Aznar A, Segond D, Rigault M, SIMOND-CÔTE E, Kunz C, SOULIE MC,
560 Expert D, Dellagi A. 2012. Iron deficiency affects plant defence responses and confers
561 resistance to Dickeya dadantii and Botrytis cinerea. Molecular plant pathology 13:816-
562 827.
563 44. Barash I, Zion R, Krikun J, Nachmias A. 1988. Effect of iron status on Verticillium wilt
564 disease and on in vitro production of siderophores by Verticillium dahliae. Journal of
565 plant nutrition 11:893-905.
566 45. Ervin E, Zhang X, Goatley J, Askew S. 2004. Trinexapac-ethyl, propiconazole, iron, and
567 biostimulant effects on shaded creeping bentgrass. HortTechnology 14:500-506.
568 46. McCall DS, Ervin EH, Shelton CD, Reams N, Askew SD. 2017. Influence of ferrous
569 sulfate and its elemental components on dollar spot suppression. Crop Science 57:581-
570 586.
571 47. Zhang S, Zhu W, Wang B, Tang J, Chen X. 2011. Secondary metabolites from the
572 invasive Solidago canadensis L. accumulation in soil and contribution to inhibition of soil
573 pathogen Pythium ultimum. Applied Soil Ecology 48:280-286.
574 48. Doornbos RF, van Loon LC, Bakker PA. 2012. Impact of root exudates and plant defense
575 signaling on bacterial communities in the rhizosphere. A review. Agronomy for
576 Sustainable Development 32:227-243.
577 49. Kamilova F, Kravchenko LV, Shaposhnikov AI, Azarova T, Makarova N, Lugtenberg B.
578 2006. Organic acids, sugars, and L-tryptophane in exudates of vegetables growing on

579 stonewool and their effects on activities of rhizosphere bacteria. Molecular Plant-Microbe
580 Interactions 19:250-256.
581 50. Pii Y, Borruso L, Brusetti L, Crecchio C, Cesco S, Mimmo T. 2016. The interaction
582 between iron nutrition, plant species and soil type shapes the rhizosphere microbiome.
583 Plant Physiology and Biochemistry 99:39-48.
584 51. Gugino BK, Abawi GS, Idowu OJ, Schindelbeck RR, Smith LL, Thies JE, Wolfe DW,
585 Van Es HM. 2009. Cornell soil health assessment training manual. Cornell University
586 College of Agriculture and Life Sciences.
587 52. Dill-McFarland KA, Breaker JD, Suen G. 2017. Microbial succession in the
588 gastrointestinal tract of dairy cows from 2 weeks to first lactation. Scientific reports 7:1-
589 12.
590 53. Kozich JJ, Westcott SL, Baxter NT, Highlander SK, Schloss PD. 2013. Development of a
591 dual-index sequencing strategy and curation pipeline for analyzing amplicon sequence
592 data on the MiSeq Illumina sequencing platform. Appl Environ Microbiol 79:5112-5120.
593 54. Weiss S, Xu ZZ, Peddada S, Amir A, Bittinger K, Gonzalez A, Lozupone C, Zaneveld JR,
594 Vázquez-Baeza Y, Birmingham A. 2017. Normalization and microbial differential
595 abundance strategies depend upon data characteristics. Microbiome 5:27.
596 55. Deng Y, Jiang Y-H, Yang Y, He Z, Luo F, Zhou J. 2012. Molecular ecological network
597 analyses. BMC bioinformatics 13:113.
598 56. Bastian M, Heymann S, Jacomy M. 2009. Gephi: an open source software for exploring
599 and manipulating networks. ICWSM 8:361-362.

600 57. Kuntal BK, Chandrakar P, Sadhu S, Mande SS. 2019. 'NetShift': A methodology for
601 understanding 'driver microbes' from healthy and disease microbiome datasets. The
602 ISME journal 13:442-454.
603 58. Rivera-Pinto J, Egozcue J, Pawlowsky-Glahn V, Paredes R, Noguera-Julian M, Calle M.
604 2018. Balances: a new perspective for microbiome analysis. mSystems 3.
605 59. Parks DH, Tyson GW, Hugenholtz P, Beiko RG. 2014. STAMP: statistical analysis of
606 taxonomic and functional profiles. Bioinformatics 30:3123-3124.
607 60. Beck MW. 2017. vif_fun.r, https://gist.github.com/fawda123/4717702. Accessed on
608 March 10th, 2020.

609

610

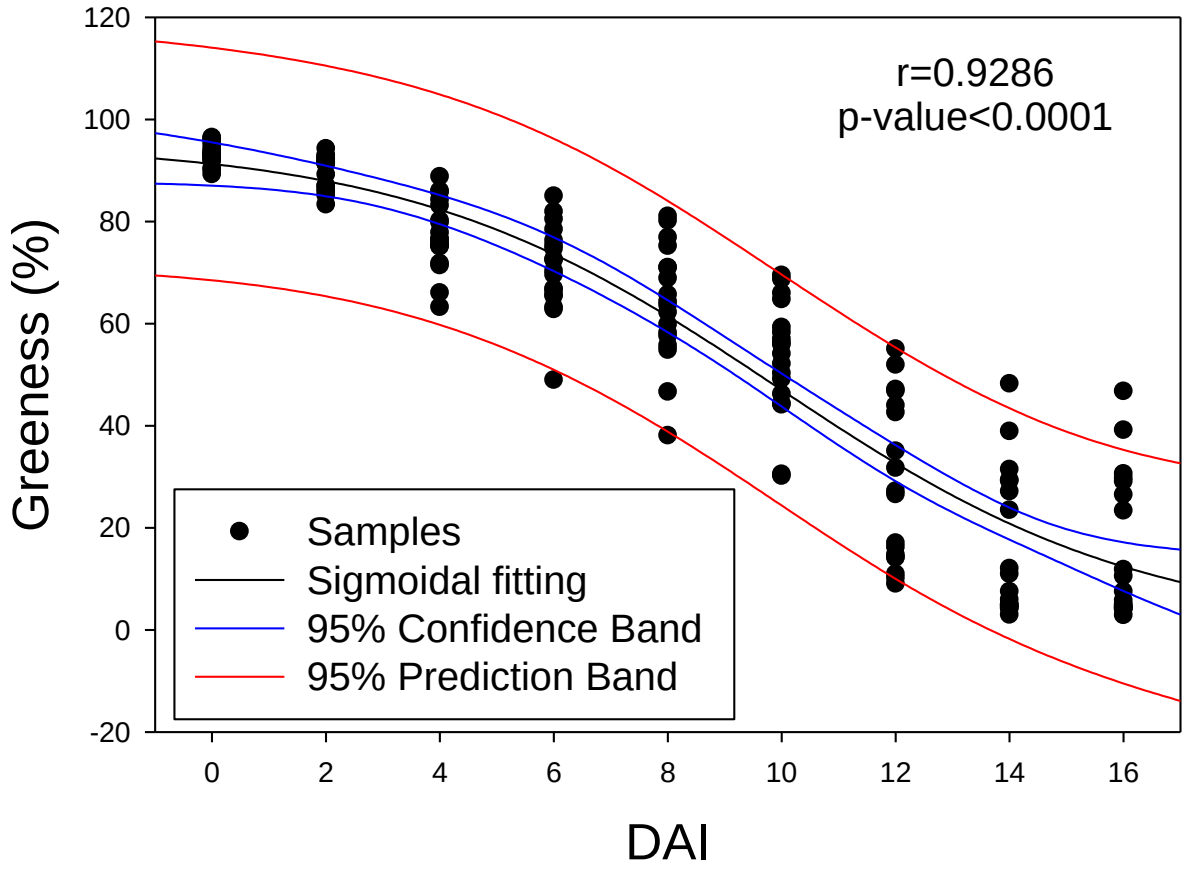

Figure 1. Dollar spot development as indicated by turf greenness decay curve fitted with sigmoidal model (r=0.9286, p<0.0001) throughout 16 days of incubation after dollar spot inoculation (n=18). DAI stands for days after inoculation with *C. jacksonii*.

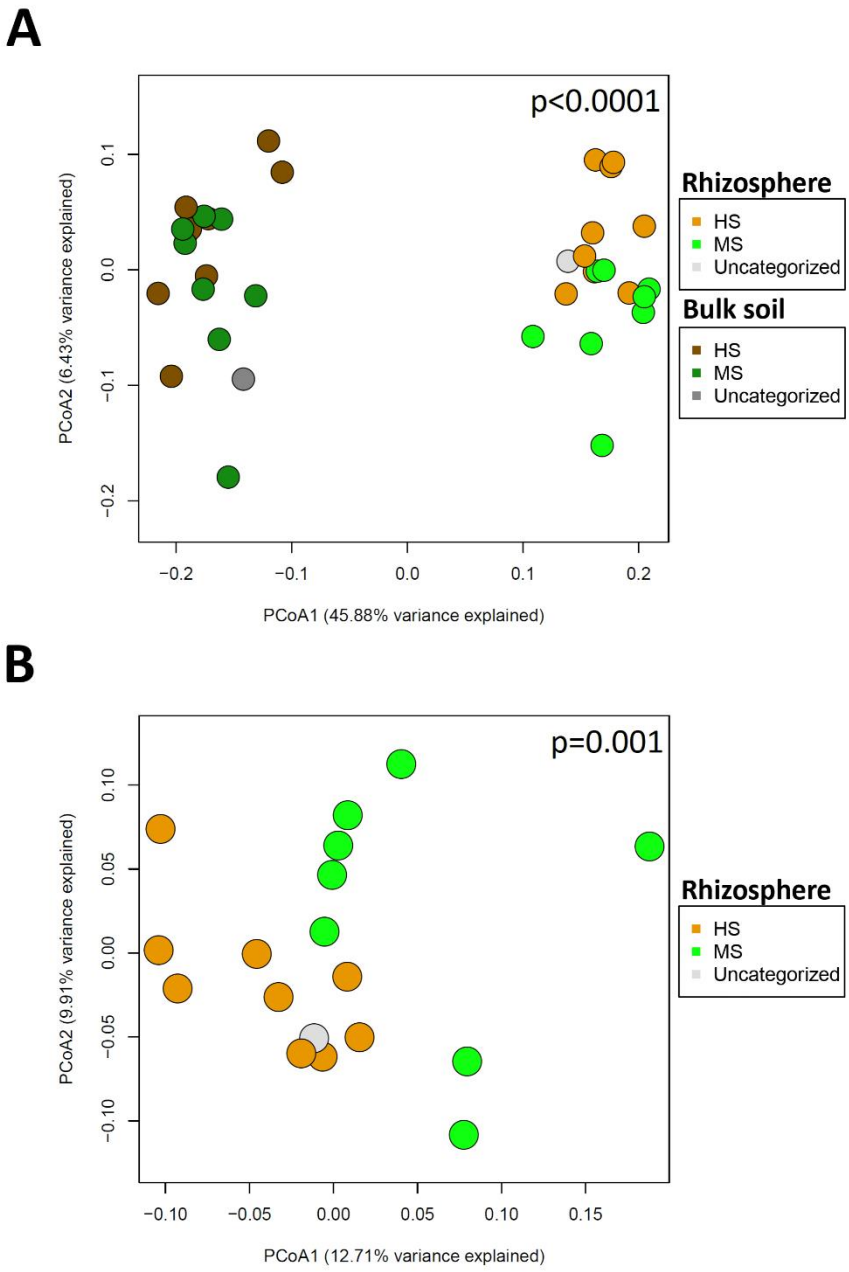

Figure 2. Principal coordinate analysis (PCoA) of bulk soil versus rhizosphere microbiome (a), and MS versus HS turfgrass rhizosphere microbiome (b). Significant differences between MS and HS samples were tested using PERMANOVA.

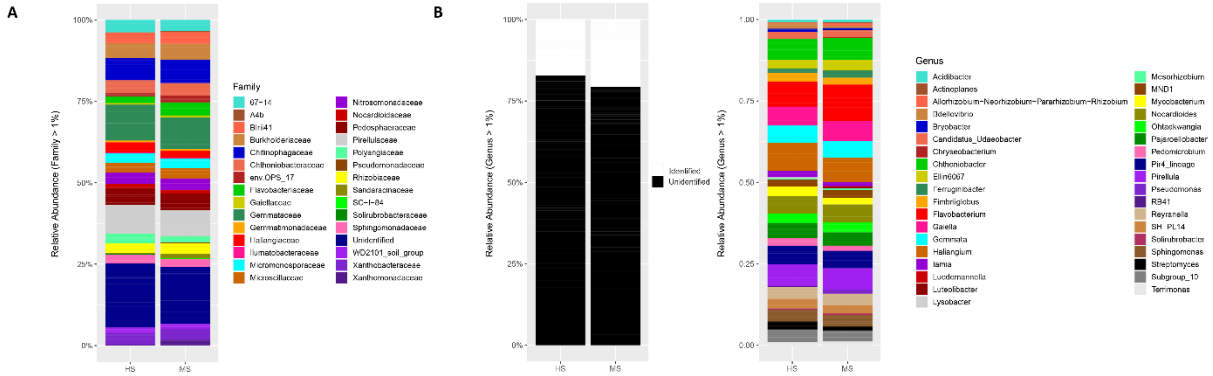

Figure 3. Relative abundance of rhizosphere microbiome from MS and HS turfgrass at Family (a) and Genus (b) level.

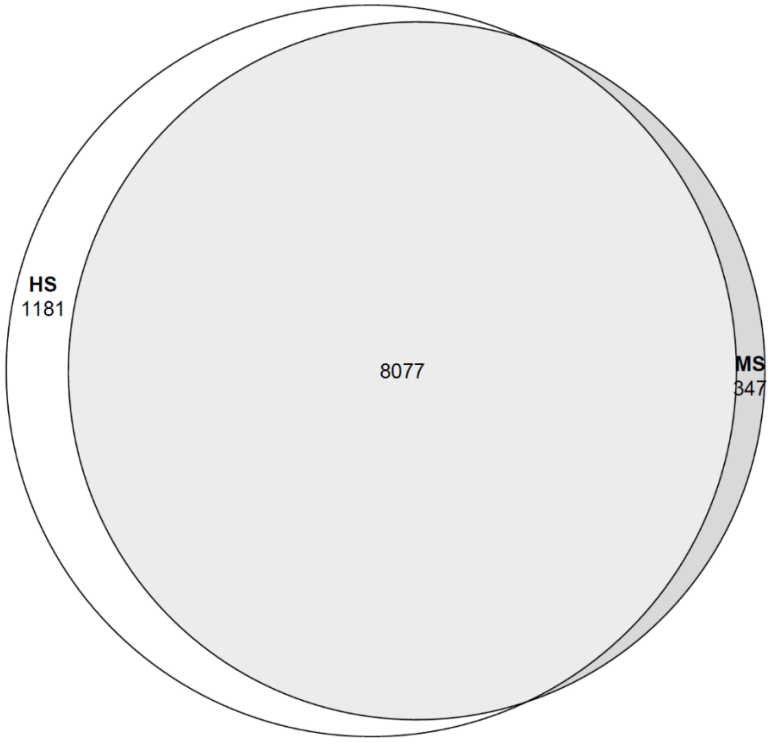

644

645 Figure 4. Proportions of shared and unique ASV between the MS and HS rhizosphere soil
646 showed as Venn diagram.

647

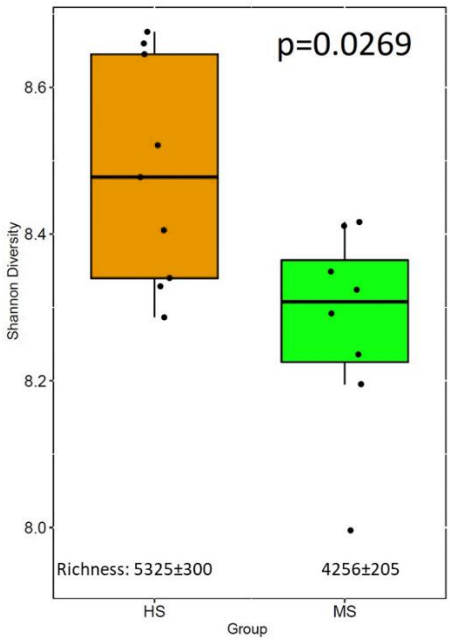

648

649 Figure 5. Bacterial Shannon diversity and richness of rhizosphere microbiome for turfgrass of
650 MS and HS susceptibility group. The Shannon diversity significant difference was performed
651 using a nonparametric Wilcoxon test.

652

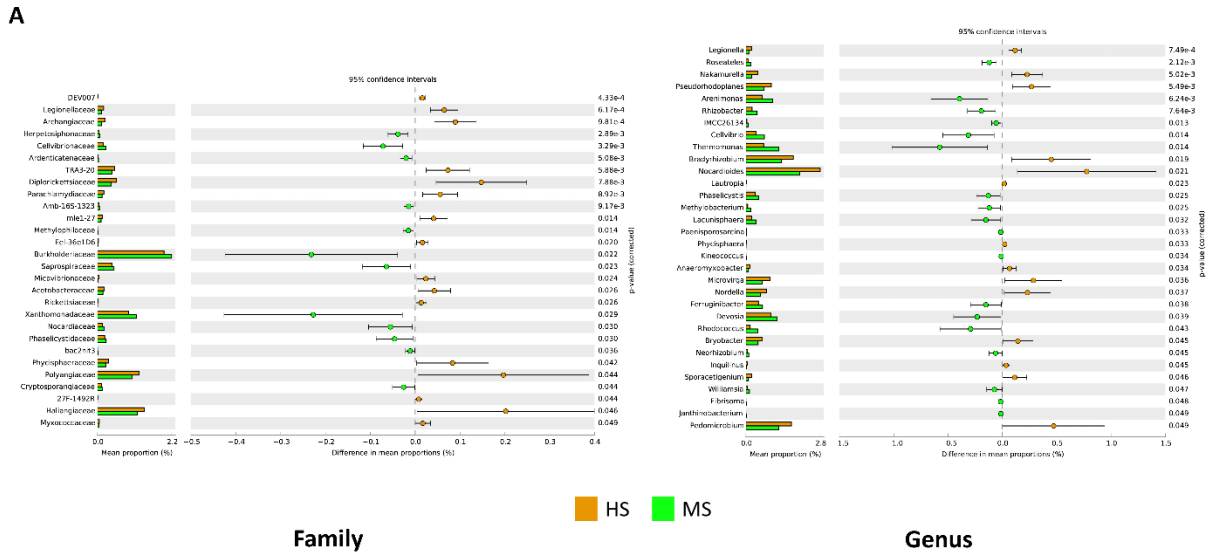

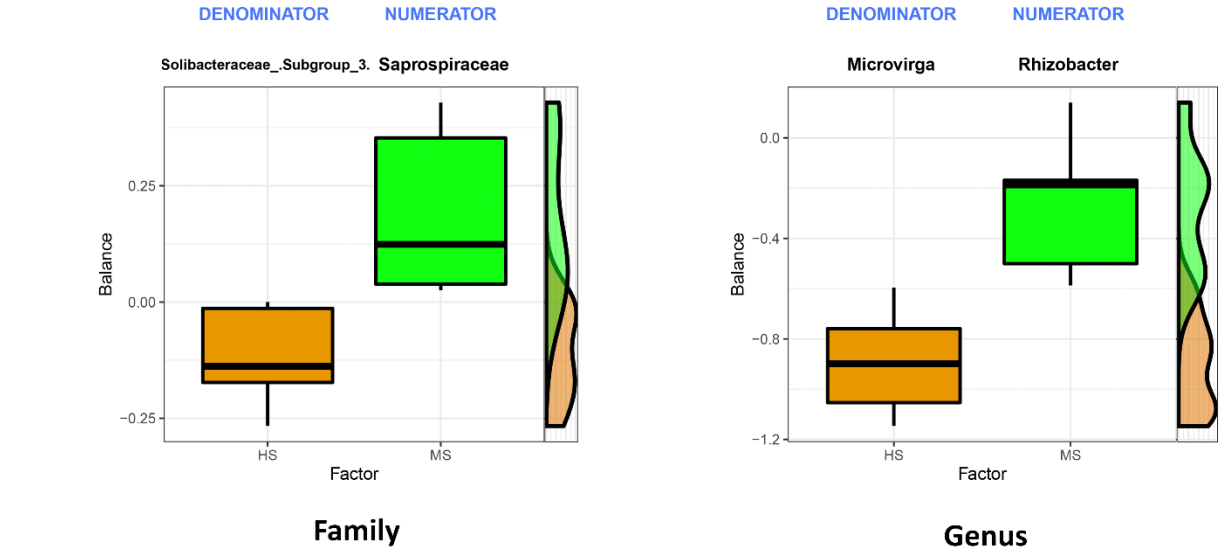

Figure 6. Rhizosphere microbial taxa relative abundance differences at family and genus level tested with Welch's t-test (a). Compositional balance change analysis identifying the microbial signatures that discriminate the rhizosphere microbiome between HS and MS (b), the balance indicates the logarithm ratio of the relative abundance of identified denominator and numerator.

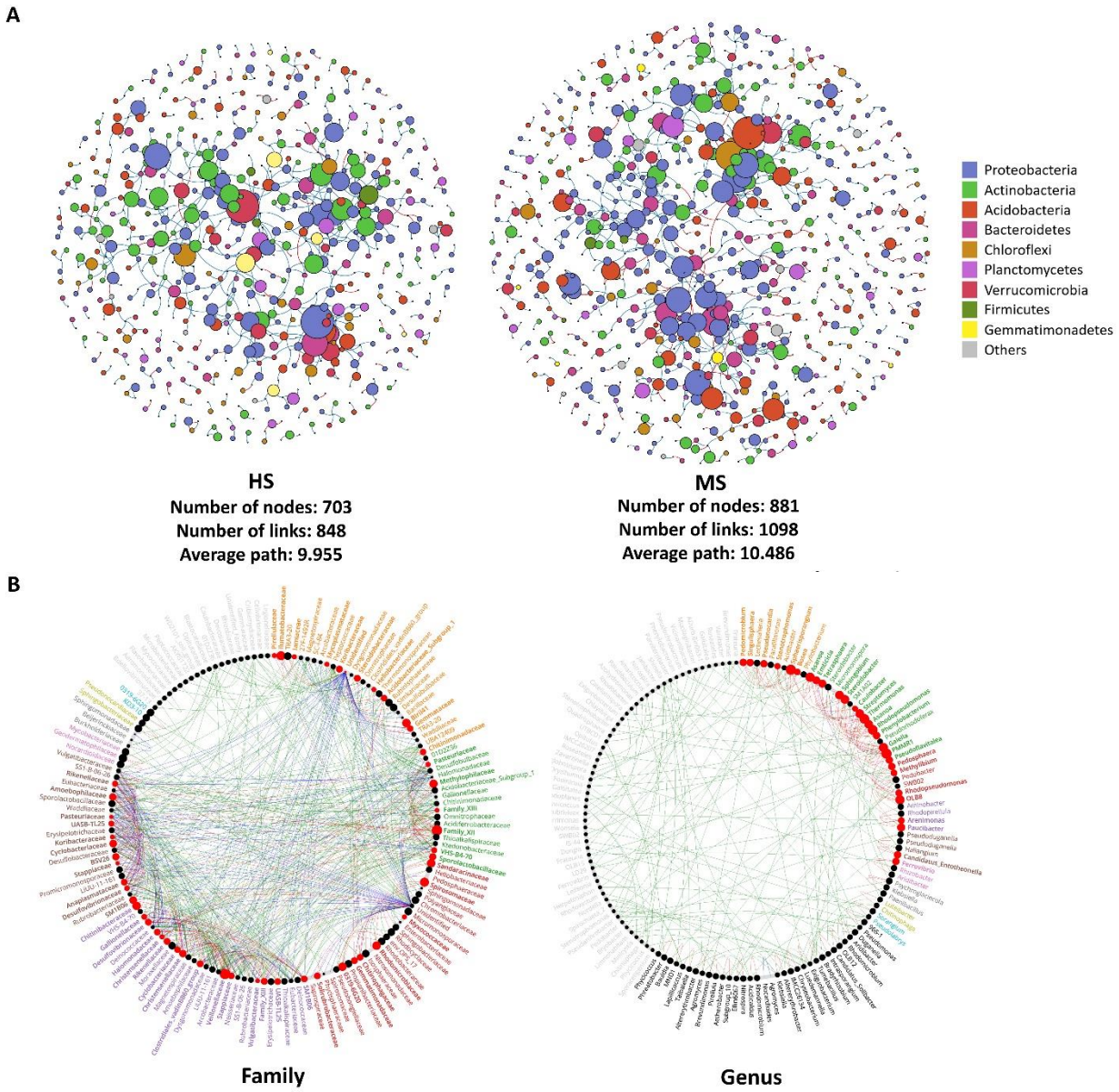

Figure 7. Rhizosphere soil bacterial microbiome co-occurrence networks at phylum level of dollar spot MS and HS turfgrass (a), in which the size of the nodes were scaled based on in-degree values, blue and pink paths represents positive and negative correlation, respectively. NetShift analysis by comparing the co-occurrence networks to identify the driver taxa at family and genus levels (b), where the nodes were scaled based on the degree in neighbor shift, the red nodes are the identified important drivers responsible for the network shift between the MS and HS turfgrass rhizosphere microbiome, and the green, red and blue paths represents the edges showed in MS, HS and both, respectively.

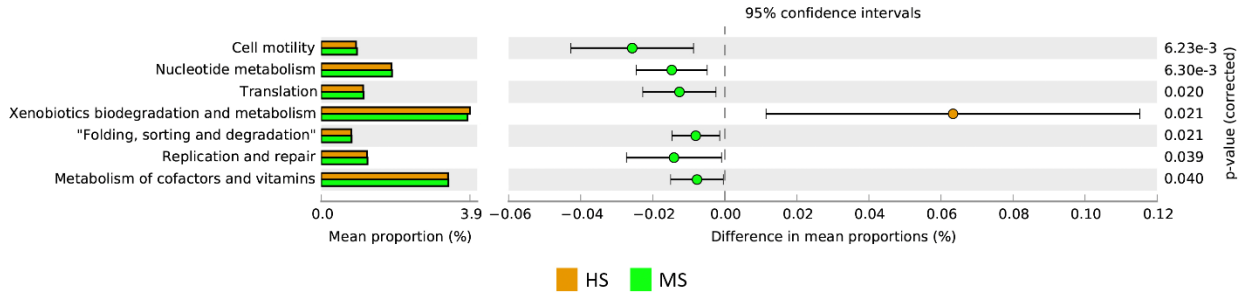

Figure 8. Significant differences in predicted rhizosphere microbiome functional pathways of MS and HS turfgrass using Tax4Fun2 and tested by Welch's t-test.

Table 1. Paired-PERMANOVA analysis of turf-associated soil microbiome prior to *C. jacksonii* inoculation as categorized based on disease level (high, medium, and low) after inoculation of *C. jacksonii* and throughout the incubation. Asterix indicates the significance level: * p<0.05 and ** P<0.01. DAI stands for Days after inoculation of *C. jacksonii*.

	Pair-comparison	0 DAI		2 DAI		4 DAI		6 DAI		8 DAI	
		R^2	P-value	R^2	P-value	R^2	P-value	R^2	P-value	R^2	P-value
Rhizosphere	High vs Low	0.116	0.126	0.124	0.090	0.138	0.006**	0.139	0.003**	0.118	0.021*
	High vs Med	0.080	1.000	0.100	0.603	0.136	0.012*	0.112	0.090	0.103	0.345
	Low vs Med	0.115	0.117	0.089	1.000	0.103	0.147	0.116	0.036*	0.096	0.807
Bulk	High vs Low	0.125	0.144	0.101	0.597	0.087	1.000	0.089	1.000	0.085	1.000
	High vs Med	0.094	0.978	0.096	0.939	0.086	1.000	0.112	0.372	0.122	0.207
	Low vs Med	0.093	0.984	0.087	1.000	0.076	1.000	0.088	1.000	0.099	0.549

	Pair-comparison	10 DAI		12 DAI		14 DAI		16 DAI	
		R^2	P-value	R^2	P-value	R^2	P-value	R^2	P-value
Rhizosphere	High vs Low	0.126	0.024*	0.091	1.000	0.091	1.000	0.091	1.000
	High vs Med	0.128	0.036*	0.080	1.000	0.096	0.840	0.096	0.816
	Low vs Med	0.109	0.096	0.092	1.000	0.100	0.540	0.100	0.573
Bulk	High vs Low	0.080	1.000	0.080	1.000	0.091	1.000	0.091	1.000
	High vs Med	0.081	1.000	0.088	1.000	0.092	1.000	0.092	1.000
	Low vs Med	0.080	1.000	0.076	1.000	0.068	1.000	0.068	1.000

Table 2. Mean separation of turf-associated bulk soil chemical elements as categorized based on disease severity (high, medium, and low) after inoculation of *C. jacksonii* and throughout the incubation (a). Iron content (mg/kg of dry soil) of each severity group categorized based on the peak of disease development stage (b). Non-parametric Kruskal-Wallis test and Steel-Dwass paired-comparison were conducted to test the significance level. Asterix indicates the significance level: * $p<0.05$ and ** $P<0.01$. DAI stands for Days after inoculation of *C. jacksonii*. Numbers followed by ± indicates standard errors.

(A)

	DAI 0		DAI 2		DAI 4		DAI 6		DAI 8		DAI 10		DAI 12		DAI 14		DAI 16	
	ChiSq	P-value	ChiSq	P-value	ChiSq	P-value	ChiSq	P-value	ChiSq	P-value	ChiSq	P-value	ChiSq	P-value	ChiSq	P-value	ChiSq	P-value
pH	0.626	0.060	4.526	0.104	3.170	0.205	1.509	0.470	1.064	0.587	2.561	0.278	2.012	0.366	2.667	0.264	2.667	0.264
OM	0.986	0.611	0.184	0.912	5.535	0.063	2.611	0.271	0.784	0.676	1.092	0.579	0.246	0.884	0.012	0.994	0.012	0.994
Al	3.942	0.139	6.398	0.041*	8.082	0.018*	5.661	0.059	4.012	0.135	9.310	0.01**	3.310	0.191	3.193	0.203	0.319	0.203
Ca	1.977	0.372	2.854	0.240	5.719	0.057	9.310	0.01**	2.561	0.278	5.485	0.064	1.450	0.484	0.889	0.641	0.889	0.641
Cu	2.117	0.347	10.714	0.005**	4.667	0.097	2.328	0.312	0.363	0.834	2.538	0.281	3.170	0.205	0.924	0.630	0.924	0.630
Fe	5.099	0.078	3.509	0.173	9.275	0.01**	7.906	0.019*	8.924	0.012*	11.614	0.003**	4.714	0.095	4.994	0.082	4.994	0.082
K	0.363	0.834	0.152	0.927	3.521	0.172	7.029	0.030	3.193	0.203	2.047	0.359	0.328	0.849	1.263	0.532	1.263	0.532
Mg	1.063	0.587	2.538	0.281	3.661	0.160	4.678	0.096	0.854	0.653	3.170	0.205	1.275	0.529	0.667	0.717	0.667	0.717
Mn	3.029	0.220	0.877	0.645	1.205	0.548	1.509	0.470	2.632	0.268	3.895	0.143	0.503	0.778	0.246	0.884	0.246	0.884
Mo	0.456	0.796	0.222	0.895	0.714	0.700	5.556	0.062	1.556	0.459	0.714	0.700	0.105	0.949	0.737	0.692	0.737	0.692
Na	1.310	0.520	0.152	0.927	4.012	0.135	3.825	0.148	0.667	0.717	3.790	0.150	0.737	0.692	0.421	0.810	0.421	0.810
P	3.240	0.198	1.368	0.505	1.298	0.523	2.246	0.325	0.877	0.645	1.064	0.587	0.714	0.700	0.573	0.751	0.531	0.751
S	1.556	0.459	0.105	0.949	0.140	0.932	0.433	0.805	0.561	0.755	0.035	0.983	2.117	0.347	2.117	0.347	2.117	0.347
Zn	1.298	0.523	3.415	0.181	0.012	0.994	0.246	0.884	1.509	0.470	1.064	0.587	0.246	0.884	1.275	0.529	1.275	0.529
C	1.064	0.587	3.193	0.203	0.667	0.717	0.246	0.884	1.450	0.484	0.012	0.994	3.193	0.203	2.538	0.281	2.538	0.281
N	1.485	0.476	2.819	0.244	0.152	0.927	1.766	0.414	1.205	0.548	0.152	0.927	3.614	0.164	2.538	0.281	2.538	0.281

(B)

	Group	DAI 4 Mean				DAI 6 Mean				DAI 8 Mean				DAI 10 Mean			
Fe	**High**	0.825	±	0.035	b	0.811	±	0.037	b	0.818	±	0.035	b	0.795	±	0.031	b
	Low	0.989	±	0.035	a	0.975	±	0.037	a	0.987	±	0.035	a	0.989	±	0.031	a
	Medium	0.859	±	0.035	b	0.887	±	0.037	ab	0.868	±	0.035	ab	0.889	±	0.031	ab

689 Table 3. Correlations among bulk soil chemical property, bulk soil microbiome and rhizosphere
690 microbiome using Mantel tests. Asterix indicates the significance level: * $p<0.05$.

Correlation	Mantel Statistic	
	R	P-value
Soil Chem vs Bulk Microbiome	-0.230	0.97
Soil Chem vs Rhizo Microbiome	0.245	0.048*
Bulk Microbiome vs Rhizo Microbiome	-0.065	0.58

691 Table 4. Stepwise selection of the optimal regression model for bulk soil chemical elements and
692 average dollar spot disease severity (greenness) during the peak disease development stage (4-10
693 DAI). Asterix indicates the significance level: *** p<0.001.

Coefficients	Estimate	Std. Error	t-value	P(>|t|)
Intercept	27.09	13.06	2.075	0.056
Fe	69.74	16.19	4.309	<0.001***
Zn	-27.28	15.81	15.81	0.105

Residual standard error: 6.011 on 15 degrees of freedom
Multiple R-squared: 0.5624,
F-statistic: 9.641 on 2 and 15 DF, p-value: 0.002031

694

695

696

697

698

699 Supplementary Table S1. Wilcoxon non-parametric comparison of soil chemical properties
700 between HS and MS associated bulk soil.

Property	Level	Mean	Std. Dev.	Std. Error Mean	Lower 95%	Upper 95%	Wilcoxon p-value
pH	HS	7.240778	0.233394	0.0777981	7.061375	7.420181	0.0543
	MS	7.398875	0.07535	0.0266401	7.335881	7.461869	
OM	HS	2.985949	0.275381	0.0917936	2.774273	3.197625	0.7361
	MS	3.076462	0.103921	0.0367415	2.989582	3.163342	
Al	HS	2.774205	0.252402	0.0841339	2.580192	2.968218	0.0161*
	MS	3.162284	0.29524	0.104383	2.915458	3.409111	
Ca	HS	1639.915	80.10273	26.700911	1578.342	1701.487	0.0433*
	MS	1714.069	110.1071	38.928753	1622.017	1806.121	
Cu	HS	0.080371	0.032808	0.0109359	0.055153	0.105589	0.2482
	MS	0.092079	0.020072	0.0070966	0.075298	0.10886	
Fe	HS	0.818683	0.097546	0.0325154	0.743702	0.893664	0.0021**
	MS	0.975093	0.055358	0.0195718	0.928813	1.021373	
K	HS	155.3454	11.78698	3.9289926	146.2852	164.4057	0.1489
	MS	161.5223	8.360104	2.955743	154.5331	168.5115	
Mg	HS	493.3613	26.29071	8.7635684	473.1525	513.5702	0.2898
	MS	507.6362	38.32882	13.551285	475.5925	539.6799	
Mn	HS	2.186369	1.367373	0.4557909	1.135313	3.237424	0.0833
	MS	3.398221	1.248337	0.4413539	2.354585	4.441857	
Mo	HS	0.005837	0.001988	0.0006626	0.004309	0.007364	0.9233
	MS	0.005627	0.001894	0.0006696	0.004044	0.00721	
Na	HS	27.50916	2.103361	0.7011202	25.89237	29.12594	0.5006
	MS	28.36482	1.818714	0.6430124	26.84434	29.8853	
P	HS	16.69933	1.557548	0.5191827	15.50209	17.89657	0.4414
	MS	15.66392	2.09468	0.7405812	13.91272	17.41511	
S	HS	4.721017	0.446798	0.1489327	4.377577	5.064456	0.5006
	MS	4.889829	0.443375	0.1567568	4.519157	5.2605	
Zn	HS	0.825432	0.158275	0.0527584	0.703771	0.947093	0.8474
	MS	0.849113	0.034658	0.0122533	0.820139	0.878088	
C	HS	1.798	0.085772	0.0285905	1.73207	1.86393	0.9233
	MS	1.843875	0.214384	0.0757961	1.664646	2.023104	
N	HS	0.170222	0.011998	0.0039992	0.161	0.179445	0.8474
	MS	0.176125	0.021649	0.0076542	0.158026	0.194224	

701

702

703

704

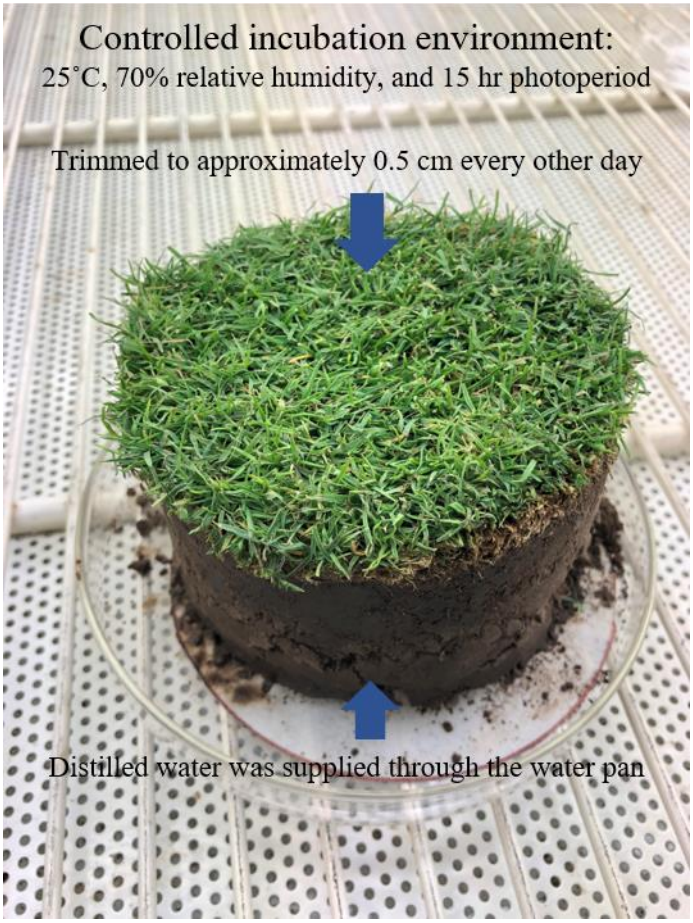

705

706 Supplementary Figure S1. Set-up of each turf sample in the controlled environment growth
707 chamber for the incubation after inoculation with *C. jacksonii*.

708

709